Flume tank testing of offshore wind turbine dynamics with foundation scour and scour protection

Russell O. Mayall[1], Ross A. McAdam[2], Richard J.S. Whitehouse[3], Harvey J. Burd[4], Byron W. Byrne[5], Steven G. Heald[6], Brian B. Sheil[7], Phillipa L. Slater[8]

[1] Doctoral Candidate, Department of Engineering Science, University of Oxford, Parks Road, OX1 3JP, UK. russell.mayall@eng.ox.ac.uk

[2] Associate Professor, Department of Engineering Science, University of Oxford, Parks Road, OX1 3JP, UK. ross.mcadam@eng.ox.ac.uk

[3] Chief Technical Director (Sediment Dynamics), HR Wallingford, Howbery Park, Wallingford, Oxfordshire, OX10 8BA, UK. R.Whitehouse@hrwallingford.com

[4] Associate Professor, Department of Engineering Science, University of Oxford, Parks Road, OX1 3JP, UK. harvey.burd@eng.ox.ac.uk

[5] Professor, Department of Engineering Science, University of Oxford, Parks Road, OX1 3JP, UK. byron.byrne@eng.ox.ac.uk

[6] Offshore Technical Support Manager, RWE Renewables UK Ltd, Greenwood House, Westwood Way, Coventry, CV4 8LG, UK. Steven.Heald@eon.com

[7] Royal Academy of Engineering Research Fellow, Department of Engineering Science, University of Oxford, Parks Road, OX1 3JP, UK. brian.sheil@eng.ox.ac.uk

[8] Technical Head, Development Offshore Wind, RWE Renewables UK Ltd, Greenwood House, Westwood Way, Coventry, CV4 8LG, UK. Phillipa.Slater@eon.com

ABSTRACT

Scour erosion processes can occur at seabed level around offshore wind turbine monopile foundations. These scour processes are often especially severe at sites where mobile sediments, such as sands, are present in the superficial seabed soils. Loss of local soil support to the monopile, caused by scour erosion, can lead to significant changes in the dynamic characteristics of the wind turbine support structure. This can result in accelerated fatigue damage due to the applied cyclic loads from the wind turbine generator, especially at the rotor frequency. Although scour erosion can be controlled by appropriate scour protection systems, there is a lack of knowledge to support the design and optimisation of these protection measures, to ensure that the dynamic performance of the wind turbine support structure remains within acceptable limits. This paper describes an experimental campaign conducted on a 1:20 scale model of a driven

monopile foundation and wind turbine support structure, founded in a prepared sand test-bed in the Fast Flow Facility flume (HR Wallingford, UK). Scour processes were induced by applying cycles of flow. Experiments were conducted to investigate the influence that these scour processes, and selected concepts for preventative and remedial scour protection, have on the dynamic characteristics of the monopile-tower system. The paper describes the experimental procedures that were adopted, and provides an assessment of the results.

INTRODUCTION

Many offshore wind turbine support structures, in operation or under development, employ monopiles with diameter D in the range 4 - 10m and embedment ratios L/D (where L is embedded length) in the range 2 - 6. Scour erosion processes, due to wave and current action, can often occur in the seabed soils around foundations, especially at sites where the superficial soil is sand-dominated. These erosion processes can cause significant loss of soil support to the foundation, with consequential reductions in stiffness and ultimate capacity. Moreover, the depth of local scour erosion holes that develop around monopiles scales with pile diameter; monopiles with larger diameters cause greater depths of local scour. The relatively large diameter but low embedment ratio wind turbine monopiles are therefore potentially vulnerable to the effects of scour.

Reductions in foundation stiffness due to scour cause corresponding reductions in the natural frequencies of the combined foundation - wind turbine support structure. This change to the dynamic characteristics of the structural system can cause accelerated fatigue damage due to the action of cyclic loads, especially those associated with the rotor frequency. Accelerated fatigue damage can lead to significant reductions in design life and asset value. In extreme cases, reductions in the ultimate capacity of the foundation, due to scour processes, may trigger concerns about the ability of the structure to operate safely within serviceability limits.

Scour processes that develop around offshore foundations are commonly categorised as (i) 'local scour' in which erosion of the soil occurs by the action of downflow and horseshoe vortices around the pile (e.g. Sumer et al., 1992), and (ii) 'general scour' in which effects such as migrating sand waves, basin-wide erosion or loss of upstream soil supply cause changes in the original sea bed level on a length scale that is considerably larger than the dimensions of the foundation (general scour is sometimes referred to in projects as leading to a change in the global seabed level). It should be noted that 'global' sedimentation can also occur, e.g. due to the passage of a sand wave crest past the pile, or due to regional accretion. An idealised

seabed profile around a monopile foundation, indicating general scour of magnitude S_G, and an additional conical local scour hole of depth S_L, is illustrated in Fig. 1.

Various approaches have been proposed to predict the depth and extent of local scour at a piled foundation (e.g. Whitehouse, 1998). Practical guidance on design values of S_L are provided in standard guidance documents (e.g. API 2011, DNVGL 2016). Recommended design values of S_L are typically proportional to the pile diameter; $S_L = 1.5D$ in API 2011 and $S_L = 1.3D$ in DNVGL 2016. Local scour equilibrium depths and development rates are influenced by the site wave and current conditions. Design values for S_G need to be determined on the basis of local site conditions, including an assessment of the way in which the seabed conditions might develop over the lifetime of the foundation.

In commercial wind farm projects, if at the design stage the risk of scour is considered to be significant, pre-installed preventative scour protection systems may be incorporated as the foundation is installed. Alternatively, when unexpected scour processes occur during the working life of a wind turbine structure, post-construction remedial scour protection systems may be employed. Rock fill scour protection - installed from a side-dump vessel or via a fall pipe - is most commonly used; and is placed either as a layer of certain thickness using a single grading or underlain with a filter layer of smaller rock. Alternative scour protection concepts such as filter units (rock-filled nets) or tyre-filled nets can be installed by lowering from a crane vessel; these offer potential cost reductions and opportunities for easier decommissioning.

Scour protection systems are primarily designed on the basis of the need to control physical scour erosion processes around the monopile, including failure mechanisms such as (i) erosion of the placed material, (ii) suction scour-induced loss of seabed sediments through scour protection layers, and (iii) instability due to secondary/edge scour at the extremity of the scour protection (e.g. Whitehouse et al., 2011; De Vos et al., 2011). Previous experimental studies on scour protection have tended to explore these hydrodynamic aspects with recent developments including: (i) allowing a 'falling apron' of rock to develop at the edge of scour protection with an unstable initial condition representing global scour (Riezebos et al., 2016), (ii) observations of sediment accumulation in suction scour tests (An et al., 2014), and (iii) observations of internal scouring adjacent to the pile wall in widely-graded scour protection systems (Petersen et al., 2019). However, there is a separate, but equally important, requirement to consider the influence of scour and scour protection systems on the structural performance of the monopile-tower system. Consideration of these structural performance issues might also provide opportunities to actively control the dynamic characteristics of the monopile-tower via appropriate scour protection systems.

This paper describes an experimental investigation on the influence of scour and scour protection systems on the dynamic characteristics of a model monopile - tower system (see summary in Mayall et al., 2018). Previous experimental work in this area, with a focus on structural performance of foundations, has been mainly limited to the influence of scour on response rather than extending to scour protection systems. Such testing typically employs artificially-generated scour holes (e.g. Prendergast et al., 2013; Prendergast et al. 2015; Qi et al., 2016), which provides a useful means of investigating idealised forms of the problem, but does not incorporate realistic aspects of actual scour erosion processes. The influence that the presence of scour protection systems has on the structural performance of monopile foundations has received limited previous attention.

The experimental campaign was conducted in the 4m wide Fast Flow Facility (FFF) flume at HR Wallingford, UK (Whitehouse et al., 2014). A model monopile - tower system at reduced scale was impact driven into a prepared sand bed in the flume test section. Water currents were employed to generate controlled scour processes around the monopile, eroding the soil in a manner representative of that at full scale in the field. The effect of these scour erosion processes on the dynamic characteristics of the monopile-tower system was assessed through dynamic testing. The influence of pre-installed rock armour scour protection, and separate remedial rock fill and tyre-filled net systems, were also investigated. The test program generated a significant amount of data, which are collated and interpreted in this paper.

It is recognised that achieving similarity between field scale structures and laboratory scale models presents difficulties due to the competing scaling of the geometric, structural, and dynamic properties of the structure, soil, fluid, and body forces. Where possible the work described in this paper has adopted appropriate scaling of geometry, structural stiffness, and mass, but it is accepted that it was not possible to achieve scaling of factors such as the mass and stiffness/viscosity of the soil and water. The data therefore support a qualitative indication of the influence that scour and scour protection systems have on the dynamic characteristics of the full scale monopile - tower systems. They provide a basis for the calibration of new scalable design models that can be applied to predict the effects of scour and scour protection systems on the dynamic performance of full-scale structures. A preliminary design model for this purpose, based on the one dimensional (1D) finite element framework, is described in Mayall et al. (2019); the experimental data presented here will be used to inform future developments of this framework.

EXPERIMENTAL SETUP

The experiments employed a sand bed prepared within a 1.0m deep and 4.0m x 4.0m plan area sediment pit located inside the FFF flume, as illustrated in Fig. 2. Initially, a 75mm thick gravel layer and a distributed perforated pipe system and permeable geotextile membrane cover were placed in the pit to provide controlled saturation and drainage. The sand bed was then built up with a fine silica sand (Bathgate psf) in 50mm thick layers using a 26kg plate compactor. Physical properties of the Bathgate sand employed in the tests are listed in Table 1.

Steel retaining beams of 100mm height, spanning across the flume width, were used to extend the height of the sand bed up to 0.7m above the flume base. A sand slope of 1:3 gradient was placed outside of the retaining steel beams to provide fairing to the flow entering and exiting the test area. Once the sand bed had been prepared, it was saturated via the distributed pipe system at a gradual rate to minimise the risk of piping.

A gloss-painted glass fibre reinforced plastic (GFRP) tube and aluminium tube were used to construct the monopile and tower sections respectively. The geometry and properties of the tube sections are listed in Table 2. The GFRP monopile was produced by CompoTech and the longitudinal modulus and shear modulus were calculated using classical lamination theory. A stiff aluminium transition piece of 0.2m length, mounted within the top of the GFRP tube, was used to provide a rigid connection between the foundation and tower. A set of brass discs were mounted on the top of the tower to represent the mass of the rotor-nacelle assembly. The number N_M of brass discs employed in the tests was varied to allow the influence of the top mass on the system dynamics to be investigated. The geometry and material of the monopile - tower structure were carefully selected to ensure similar physical behaviour to full scale structures using the dimensionless groups described in Table 3. The dimensionless properties were compared against two datasets for full scale structures; (i) Robin Rigg offshore wind farm in the UK (data supplied by E.On Energy), and (ii) using wind turbine parameters compiled by Arany et al. (2016) for ten offshore wind farms across the Netherlands, Belgium and UK. Further detail on the typical loading and structural natural frequencies of varied scale offshore wind turbines can also be found in Arany et al. (2016).

Dynamic tests were conducted by exciting the structure with a finger tap on the tower at z = 5.47m, above the pile tip. The applied force was measured using a PCB Piezotronics 208C01 type IEPE force sensor. The response of the structure was measured in the streamwise and crossflow directions at six positions along the tower using twelve PCB Piezotronics 333B50 type IEPE uniaxial accelerometers. The accelerometers were

mounted on cruciform brackets inside the tower section (see Mayall et al., 2018). All test control and data acquisition processes were carried out using National Instruments compact DAQ instrumentation. The masses and locations of the peripheral pile/tower assembly components, including the force sensor and accelerometers are listed in Table 4.

TEST MATRIX

Six tests were performed to explore the influence of various global scour, local scour and scour protection systems on the dynamic characteristics of the model monopile – tower system. Table 5 lists these tests, including the target depths of local and global scour and the generic forms of the scour protection systems that were applied. The scour depths actually achieved in the tests varied from these targets, and is discussed later in the paper. The following common routine was adopted for the testing programme:

1. Prepare sand bed.
2. Conduct cone penetrometer tests.
3. Install preventative scour protection (Test 5 only).
4. Fill flume to target water depth.
5. Drive pile to target depth.
6. Develop local scour via two-way water flow.
7. Install remedial scour protection (Tests 2,3,4,6 only).
8. Develop global scour by incremental removal of steel retaining beams and two-directional water flow.
9. Conduct lateral monotonic loading test (outside scope of current paper).
10. Drain flume
11. Inspect the scour protection condition (Tests 2 to 6)

Test 1 did not employ a scour protection system; it therefore provided a scour-only reference case.

SAND BED CHARACTERISATION

Cone penetrometer testing

Cone penetrometer tests (CPT) were conducted on the prepared sand bed, at the centre of the pile installation location, after the sand had been saturated. This provided a check on the repeatability of the bed preparation process as well as data to support future modelling exercises. A cone 8 mm in diameter with 60° angle cone tip was employed, with load measurements at the cone tip and the jacking point. The rate of cone advance was 4 mm/s. Fig. 3(a) shows the depth variation of the measured cone end bearing, q_c for all of the tests. A separate calibration exercise was conducted using samples of saturated Bathgate sand at known

178 relative density D_R to obtain the correlation (based on a previously-suggested form e.g. Jamiolkowski et al.,
179 1985):

$$D_R\ [\%] = -37.53 + 23.97 \ln \frac{(q_c/p_{ref})}{(\sigma'_v/p_{ref})^{0.5}} \quad (1)$$

180 where the reference stress is p_{ref} = 100 kPa and σ'_v is the initial vertical effective stress in the soil at the level
181 of the cone tip.

182 The variation of relative density with depth for each test, on the basis of the correlation in Equation (1), is
183 plotted in Fig. 3(b), which can be applied within numerical and design methodologies, such as the PISA
184 design model (Burd et al., 2019).

185 *Small strain shear modulus*

186 The initial lateral resistance of the pile is likely to be highly dependent on the shear stiffness of the soil.
187 Various published correlations between CPT end bearing and small strain stiffness can be chosen (e.g. Rix
188 and Stokoe, 1991; Baldi et al., 1989), which result in significant variance in the derived stiffness. In order to
189 address this uncertainty, data on small strain shear modulus (G_0) were measured in bender element and
190 resonant column tests of known relative density (Table 6) performed by Fugro, Wallingford, UK.

191 G_0 was measured in the bender element tests for isotropic stress conditions at values of mean effective
192 stress, p', in the range 5 kPa to 50 kPa, and in the resonant column tests at mean effective stresses of
193 between 10 kPa and 50 kPa. Data are shown in Fig. 4. It is clear that G_0 increases significantly with stress
194 level; there is also a small apparent dependency on relative density.

195 These shear modulus data can be represented to a reasonable accuracy using $B = 478$ in the Hardin and
196 Richart (1963) correlation,

$$G_0 = \frac{B p_{ref}}{0.3 + 0.7e^2} \left(\frac{p'}{p_{ref}} \right)^{0.5} \quad (2)$$

197 where p' is mean effective stress and p_{ref} = 100 kPa. This correlation is indicated on Fig. 4 and the inferred
198 variance of small strain stiffness for the tests are shown in Fig. 3(c), where it has been assumed that the
199 mean effective stress can be approximated by the vertical effective stress (i.e. K_0 = 1). Little difference is
200 observed between the small strain stiffness profiles for each test, with Test 1 presenting the lowest cone tip
201 resistance and resulting stiffness, likely due to small variations in the bed preparation process. However, the
202 analysis of measured natural frequency (see Fig. 13) does not indicate any subsequent influence and the
203 repeatability of the sand bed preparation is therefore considered sufficiently consistent.

It is recognised that the pile driving process is likely to result in changes to the soil stresses and density local to the pile, and the resulting soil stiffness (Jardine et al., 2005). However, further research is required to assess the lateral extent of these changes and their impact on the small strain behaviour of monopiles under dynamic loading.

Soil friction angle

Triaxial compression tests were conducted in undrained conditions on BE1 and drained conditions on BE2, see Table 6. The critical state triaxial compression friction angle was determined as 34.3^{o} from these tests.

FOUNDATION INSTALLATION

The fully assembled monopile and tower was impact driven into the prepared sand bed to a tipping depth of $3D$ above the sand bed base (H_B = 600mm in Fig. 2) using a 7.75kg annular drop weight applied to a polyethylene cushion on top of the monopile. The selected drop weight and height was found to achieve a penetration rate of at least 0.25 mm per blow during trials performed prior to the FFF experiment campaign. The soil plug length z_{plug} was measured by a plumb line lowered through a hole in the transition piece. The total driving energy was calculated as the product of the hammer weight, hammer stroke, and number of blows.

Fig. 5 shows the cumulative number of blows, hammer drop heights, and driving energy applied during installation; Table 7 lists the length of the soil plug at the end of driving for each test. In all cases there was drawdown of the soil inside the pile. The increased blow count and associated total energy for Test 2 resulted in a refinement of the strategy for the driving of subsequent tests, to move to longer hammer strokes at lower blow counts, resulting in the consistent profiles of blow count and driving energy for subsequent tests. In Test 3 it was found that the pile had twisted during driving and was misaligned by 7° anticlockwise (viewed from above) about the vertical axis at the end of driving.

FLOW REGIME FOR SCOURING

An approximately square wave pattern of reversing flow was used to simulate a tidal current for the development of local and global scour, as illustrated in Fig. 6. Current speeds were selected on the basis of sediment transport scaling, to represent live-bed conditions in the field (i.e. where sediment transport occurs generally across the seabed). The FFF allows recirculation of suspended sediments to allow representative modelling of live bed conditions, including a replenishing upstream sediment supply. Depth averaged current

velocities ($\overline{U}$), measured using an acoustic Doppler current profiler, exceeded the critical threshold of sediment motion ($\overline{U}_{crit}$) of 0.3 m/s, calculated using Equation 3 (Soulsby, 1997).

$$\overline{U}_{crit} = 7\left(\frac{h_w}{d_{50}}\right)^{\frac{1}{7}}\left[g(G_s-1)d_{50}f(D_*)\right]^{1/2} \quad \text{For } D_* > 0.1 \qquad (3)$$

$$f(D_*) = \frac{0.30}{1+1.2D_*} + 0.055[1-\exp(-0.02D_*)]$$

$$D_* = \left[\frac{g(G_s-1)}{\nu^2}\right]^{\frac{1}{3}} d_{50}$$

where ν is the kinematic viscosity of fresh water used in testing, assumed to be 1.23x10^{-6} m^2/s for 12°C.

The adopted phases of flow are listed in Table 8. Phase 1 indicates the conditions employed to develop local scour, and Phase 2 specifies the flow processes employed to develop global scour. The morphodynamics for Phase 1 was selected using local scour prediction methods (Whitehouse, 1998). Phase 2 was designed on the basis of sediment transport considerations (Soulsby, 1997) both to increase the overall sediment transport rate in the test section and to generate bed lowering through net loss from the test section.

LOCAL AND GLOBAL SCOUR ANALYSIS

The bathymetry local to the pile and scour hole was measured periodically during the tests using an underwater laser scanner (ULS), with a typical spatial resolution of approximately 0.001 – 0.003m. The scanner was mounted on a traverser located at y = 0.3m, see Fig. 7(a). Fig. 7(a) also shows a typical plan layout of bathymetry obtained from the ULS system.

The local bed level, (i.e. the level adjacent to the pile), used to define the total scour depth S_T, was determined as the median of the data for 0.5 ≤ r/D ≤ 0.75, where r is radial distance from the pile centre. The global bed level, used to establish the global scour depth S_G, was determined as the median of the data for 4.5 ≤ r/D ≤ 7.5, as shown in Fig. 7(b). To account for shadowing effects of the pile on the ULS measurements, only data for $y \geq 0$ were considered. Symmetry of the bed levels about $y = 0$ was assumed for the median and percentile calculations described later. Based on the bathymetry comparison for $y \geq 0$ and $y \leq 0$ on Fig. 7(a) this is shown to be a reasonable assumption. Scour depths were determined relative to the global bed level at the start of each test.

The scour depths for each test, determined using the procedures outline above, are listed in Table 9. These data are presented in terms of total scour and global scour (rather than local scour) since total scour

is measured more directly than local scour. The local scouring process produced repeatable results in terms of depth of fully-formed local scour holes (Tests 1, 2, 3, and 6). It is noted that the Phase 1 flow process induced a small amount of unintended global scour as indicated in the table. The global scour depths achieved in the tests were significantly less than the target values (specified in Table 5 based on values observed in the field). The discrepancy between target and achieved global scour was due to the experimental difficulty in naturally removing sand from the test section by sediment transport. Since the tests were in the live bed regime there was loss of sediment at the test section as well as replenishment on reversing flow cycles.

The actual value of global scour achieved was greatest in Test 6 when, as noted below Table 8, the flow time series was modified to increase the lowering. In the earlier tests even though smaller than target global scour had been achieved it was important to keep a consistent approach so that the effects of other parameters could be evaluated. The obtained local and global scour provide sufficient range for the purpose of the current study.

INSTALLATION OF SCOUR PROTECTION SYSTEMS

Three types of scour protection system were investigated: pre-installed rock armour, remedial rock fill and remedial tyre-filled nets.

Fig. 8 illustrates the geometric definitions adopted to characterise these scour protection systems, including geometries before and after further scour erosion. Note that when scour protection is present, the total scour depth S_T is defined with respect to the level of the scour protection adjacent to the pile. This is in contrast to schemes for the case where scour protection is absent, illustrated in Fig. 1.

For Test 2 the configuration of the tyre-filled nets (TFNs) was specified to match that installed for five monopiles at Scroby Sands offshore wind farm in the UK (data provided by E.On Energy). Two rings of six tethered TFNs were lowered into position in the local scour hole Fig. 9(a). The TFNs consisted of nylon mesh bags filled with 50 rubber model truck tyres (Italeri 1:24 scale model 3889 truck rubber tyres, G_S = 1.2, outside diameter = 42mm, inside diameter = 26mm, tread width = 11mm, wall thickness = 1mm).

The selected scour protection rock material consisted of an angular narrow-graded limestone gravel of median diameter d_{50} = 18.3mm with G_S = 2.8 (re-analysed since Mayall et al., 2019); the density of the rock is similar to the 'normal' density rock used offshore and sometimes 'high' density rock is used where G_S ~ 3, . The rock scour protection grading curve was selected from those available for geometric similarity to that

installed at selected full size structures at Robin Rigg offshore wind farm (data provided by E.On Energy); Fig. 10 presents a comparison of the full scale and experiment scale rock grading curves.

For Tests 3, 4 and 6, the limestone gravel (representing rock fill material for scour protection) was placed underwater using an inclined fall pipe as shown in Fig. 9(b), with its opening located close to the surface of the scour hole to facilitate placement accuracy. The fall pipe simulates rock installation in the field and removes the risk of any operator induced bed disturbance which would change the stress field. From observations during rock installation the rocks embedded about 20% of their diameter in the sand bed and the target thickness of rockfill was between 2/3 and 3/4 of the local scour hole depth.

For Test 5, the limestone gravel was placed immediately following the bed preparation using a template with geometry defined in Fig. 8(a) and edge slope of rock 1V:3H. This was intended to represent a pre-installed scour protection configuration. Fig. 9(c) shows the pre-installed rock after placement. A thin steel retaining collar was used for Test 5 only to create a small annular space between the rock and pile wall and hence prevent damage to the pile during driving; the collar was removed prior to flow Phase 1.

Table 10 lists the installed characteristics of the scour protection system employed for each test. The width b (Fig. 8) was estimated from the post-installation bathymetry plots. The in-place dry density of the scour protection material ρ_d was calculated using the installed mass of material and the volume of the scour protection material determined from the bathymetry measurements. The bulk voids ratio e and porosity n for the scour protection material were calculated from the dry densities using standard methods (e.g. Craig, 1992). The installed scour protection material has a lower density and higher voids ratio than the original sand that has been scoured.

STRUCTURAL DYNAMICS MEASUREMENTS

Measurements of the dynamic response of the monopile - tower system were conducted during scheduled pauses in the flume flow (i.e. with standing water), concurrent with bathymetry measurements. In the pause periods the number of top masses was varied. After each change the structure was excited with a finger tap impulse applied to the mounted force sensor (close to the tower top), with signals allowed to decay naturally. Data were sampled at a frequency of 3012Hz logged for 32s periods.

Fig. 11 shows a typical measured acceleration signal and the corresponding power spectral density (PSD); this indicates first, second and third mode peaks in PSD at frequencies of 6.6, 19.7 and 48.6Hz; these peaks are close to but not identical to the natural frequencies due to the influence of damping. For

each test a minimum of three impulses were logged in each of the streamwise (x-axis) and spanwise (y-axis) directions.

Values of the first three natural frequencies and corresponding mode shapes and modal damping ratios, were determined from the measured acceleration time series starting 0.5s after the peak measured force. It was assumed that the modes were uncoupled, and that each mode could therefore be considered as a single degree of freedom system:

$$\ddot{v}_m(t) + 2\zeta_m \omega_{n,m} \dot{v}_m(t) + \omega_{n,m}^2 v_m(t) = 0 \quad (4)$$

where $v(t)$ is the displacement at an arbitrary point on the tower, $\omega_{n,m}$ and ζ_m are circular natural frequency and damping ratio respectively for the m^{th} mode.

For damped free vibration, the solution for the displacement is

$$v_m(t) = v_{0,m} e^{-\zeta \omega_{n,m} t} \sin(\omega_{n,m} \sqrt{1-\zeta_m^2}\, t + \phi_m) \quad (5)$$

where $v_{0,m}$ is a constant (that depends on the initial conditions), and ϕ_m is a phase angle.

The data were initially smoothed to remove high frequency noise, using a moving average method with window length of 30, and linear trends were removed. Values of $\omega_{n,1}$ and ζ_1 were then determined by fitting the model in Equation (5), by least squares, to each accelerometer data, adopting sample lengths of approximately 20 cycles. Values of $\omega_{n,1}$, ζ_1 and $\phi_1$were common, whilst v_1 varied between accelerometers. The distribution of v_1 along the tower was used to determine the mode shape. Moving average filters were more consistent in fitting results to Equation (5), (when compared to alternatives, such as Savitzky-Golay filters) and were selected as the preferred approach.

After fitting the first mode, the residual acceleration signals were calculated by subtracting the first mode signal estimated from the model, and further linear detrending. A similar fitting process to that adopted for the first mode was then conducted on the residual accelerations to determine $(\omega_{n,2}, \zeta_2)$. The process was then repeated to determine the third mode data $(\omega_{n,3}, \zeta_3)$. Example data obtained from this procedure are shown in Fig. 12 in terms of natural frequency $f_{n,m}$, where $f_{n,m} = \omega_{n,m}/2\pi$. The mode shapes are presented using the normalisation $V_0/|V_0|_{max}$ as indicated in Fig. 12(d), this is the accepted method of presenting mode shapes in modal analyses (for the example shown in Fig. 12(d), in the case of modes 1 and 2 $|V_0|_{max}$ occurs at the same location z = 5.5 m, in the case of mode 3 this is at a different location z = 3.6 m).

For each top mass and vibration mode, the natural frequency was inferred as the mean fitted value across multiple impulse taps from both streamwise and spanwise directions. The inferred natural frequency

342 and damping ratio of the first, second and third modes are plotted in Fig. 13 at the start of each test (un-
343 scoured conditions) for all values of top mass M_{Top} (Table 4) where M_{Top} includes the brass top mass discs,
344 force sensors and mounting.

345 Fig. 13 shows that, as expected, there is a tendency for the natural frequencies to reduce with increased
346 top mass. This effect is particularly marked for the first mode. Data for the second and, to a lesser extent the
347 third mode, exhibit a certain amount of variability. This is a likely indication that these modes are especially
348 sensitive to the soil conditions such that minor difference in the stiffness of the prepared sand bed have a
349 significant effect on the natural frequencies. Test 5 has the pre-installed rock armour scour protection and
350 Test 6 has a larger initial pile embedment.

351 **EXPERIMENTAL RESULTS**

352 *Unremediated scour development; Test 1*

353 Fig. 14(a) shows the measured global and local levels throughout Test 1 (in which scour protection
354 systems were absent). During flow Phase 1 a significant amount of local scour, accompanied by some
355 unplanned global scour, develops. In Phase 2, the global scour is seen to continue. A small rise in the local
356 scour level is apparent at T_f = 25 hours suggesting that the scour hole had been partially backfilled by
357 deposited sand, presumably caused by a sand wave moving through the test area during the global lowering
358 process.

359 Changes in the inferred first three natural frequencies (relative to the un-scoured conditions) are plotted in
360 Fig. 14(b). It is interesting to note that the second mode natural frequencies exhibits the greatest sensitivity
361 to local scour; indeed the rise in the local scour level at T_f = 25 hours is concurrent with a peak in the second
362 mode natural frequency.

363 *Remedial tyre-filled net scour protection; Test 2 (R-TFN)*

364 The variations of bathymetry and natural frequency during Test 2, in which tyre-filled nets were installed
365 in a fully-developed local scour hole, are shown in Fig. 15. The natural frequencies show negligible change
366 when the tyre-filled nets were initially placed, shown in Fig. 16 for the first mode. This is attributed to the low
367 stiffness and bulk density of the tyre-filled nets relative to the undisturbed sand.

368 The variability of local bed level measurements immediately after installing the tyre-filled nets (5^{th} and 95^{th}
369 centiles) is greater than that seen in rock fill remedial scour protection tests (discussed in subsequent
370 sections). This is due to the presence of gaps between the nets and varying levels of the nets around the
371 pile. The local levels reduced by about $0.5D$ in the global scour flow phases; this is associated with

372 settlement and deformation of the tyre-filled nets. During these global scour phases there was no significant
373 further local scour compared with Test 1, and the natural frequencies remained relatively unchanged.
374 Examination of the tyre-filled nets at the end of the test indicated that sand had accumulated in them to
375 various degrees, with some nets sitting on the soil surface, some partially buried, and some fully buried, as
376 shown in Fig. 17.
377 *Remedial rock fill scour protection; Tests 3 (R-RF1), 4 (R-RF2) and 6 (R-RF3);*
378 Remedial scour protection in the form of rock fill in the locally scoured hole was installed in three tests. In
379 Tests 3 and 6, rock was installed in a fully-formed scour hole. In Test 4 rock was installed in a partially-
380 formed scour hole, resulting in a thinner deposit of rock.
381 Fig. 18(a),(c)&(e) show the measured local and global bathymetry during the three tests. The first three
382 natural frequencies generally show a step increase after installing scour protection (Fig. 18(b),(d)&(f)), with a
383 small relative change observed for Test 4 (R-RF2), in which the remediation of a shallower scour hole has
384 less influence on the natural frequency recovery. The frequencies corresponding to the equivalent
385 embedment in undisturbed sand were not fully recovered, shown in Fig. 19 for the first mode. Fig. 20 shows
386 excavated cross-sections through the scour protection material at the end of each test. These excavations
387 were performed after the pile had been subjected to monotonic loading to failure; the pile is therefore
388 displaced from the original position.
389 During the global scour phases in Tests 3 and 6, the local bed level remained stable. In Test 3 and 6 the
390 natural frequencies increased in the initial global scour phases ($8 < T_f < 25$), and approach the natural
391 frequencies of the equivalent scour depths during local scouring Fig. 19(a & c). This rise in natural frequency
392 is considered to be due to sand accretion in the rock matrix. Fig. 20(a & c) show that at the end of the tests
393 the rock matrix is seen to be packed with sand. The process by which this sand accretion occurs was not
394 directly observed during the tests.
395 Continued flow in Phase 2 of Tests 3 and 6 induced further global scour and resulted in reducing natural
396 frequencies. Since the local bed level was stable, this suggests that changing surcharge from the global bed
397 level has influenced the scour protection stiffness contribution.
398 In Test 4, where scour protection was placed in a partially-formed scour hole, the local pile embedment
399 gradually reduced during global scour flow phases as the scour protection material was consumed by
400 formation of a falling apron, and the rock level at the pile wall was lowered as shown in Fig. 18(c) and

observed in the excavations in Fig. 20(b). This loss of support around the pile caused a reduction in the natural frequencies shown in Fig. 18(d).

Considerable accretion of sand in the rock matrix was observed in all cases (Fig. 20). This infilling may be due to the combined effects of deposition at the ground surface and from suction scour of the sand beneath the scour protection. However, the base of the scour protection material in excavations of Tests 3 and 6 was observed to be unchanged since installing the rock, suggesting sand deposition due to the high sediment supply in the live-bed test conditions was the dominant process (supported by results of An et al., 2014).

It was observed in all cases that sand accretion did not occur in the rock material close to the pile wall near the surface. This local absence of accreted sand, apparent in all of the images in Fig. 20, is considered to be due to local horseshoe vortex action around the base of the pile.

Falling aprons of scour protection material were observed in Tests 4 and 6, indicating a dominant erosion of the underlying sand at the periphery of the scour protection. The falling aprons were typically one to three stones in thickness; the edges of the scour protection material and the falling aprons were partially buried by sand bedforms. The thickness of the scour protection layers was predominantly maintained throughout the global scouring stages of Test 3, as shown in Fig. 21. However, the development of significant falling aprons and the transport of rock away from the pile resulted in reductions in scour protection thickness for Tests 4 and 6, most significantly for the partially filled scour hole of Test 4.

Excavations following Test 4 indicated that the base of the scour protection layer had lowered by $0.46D$, and the thickness of scour protection material at the pile wall had reduced by 39%. It is possible that suction scour may have caused settlement of the scour protection in Test 4, after most of the rock had been depleted by formation of the falling apron.

Pre-installed rock armour scour protection; Test 5 (P-RA)

During the flow cycles that followed the pre-installation of rock scour protection (Test 5) there was negligible change in the bathymetry levels close to the pile wall at all test stages, as shown in Fig. 22(a). However, a moderate increase in the natural frequencies is observed in Fig. 22(b). indicating some stiffening of the soil-structure interaction, possibly due to the effect of sand accretion in the scour protection layer. Following the global scour phases, a falling apron developed at the toe of the scour protection, and rock infilled with sand was observed during excavation at the end of the test shown in Fig. 23. Similar to Tests 3, 4 and 6 excavations (Fig. 20) a zone of rock near the pile wall remained clear of sand. In the current case,

430 the competing effects of the sand accretion and falling apron formation appear to have a net effect of
431 marginally increasing the natural frequencies.
432 At the end of the test a small depression was observed in the level of scour protection close to the pile
433 wall (Fig. 23). This feature appears to relate to pile installation processes rather than being caused by scour.
434 **DISCUSSION**
435 An experimental campaign is described in which the influence of scour erosion, and scour protection
436 systems, on the dynamic characteristics of a reduced-scale monopile-wind turbine support system is
437 investigated. Scour processes were modelled by conducting the tests in a flume, employing two-way flow to
438 represent tidal cycles and live-bed scour, where global scour development was initiated mid flume test. A
439 consequence of this approach (instead of alternative procedures in which scoured bed profiles are formed
440 artificially) was that the scoured bed profiles exhibited considerable spatial variability (as it would in reality).
441 The complexity of the bathymetry data necessitated a detailed and careful analysis to infer appropriate
442 characteristic dimensions for the scoured seabed, to support an analysis of the dynamic test results.
443 Since the global scour is created by flow during the test (rather than by an initial unstable condition, e.g.
444 in Riezebos et al., 2016) the current experiments are considered to incorporate a degree of realism that is
445 absent in alternative experimental approaches involving artificial seabed and scour protection profiles. The
446 'live bed' conditions employed in the tests induced various complex interactions involving the accretion of
447 sand in the scour protection systems and 'falling apron' deformations of rock scour protection material.
448 These interactions are consistent with other laboratory studies (Arboleda Chavez et al., 2019 and Riezebos
449 et al., 2016) and presumed to be representative of field conditions. Field data presented by Hucker et al.
450 (2019) shows natural frequency increases over time for wind turbines with scour protection installed in
451 mobile sandy seabeds potentially due to settlement and densification of the scour protection and, in our
452 view, sediment accretion.
453 Tests conducted for cases where scour protection systems were absent allowed the influence of scour
454 processes on the dynamic performance of the system to be observed in isolation. Scour processes were
455 observed to significantly reduce the first three natural frequencies of the monopile-tower system. Reductions
456 in the first natural frequency have a particular practical significance for working wind turbine structures,
457 because of concerns that excessive accumulation of fatigue damage might occur if the first natural frequency
458 were to drift into the turbine rotor frequency band. The results demonstrate that the second natural frequency
459 is especially sensitive to scour effects, which is broadly in agreement with published numerical studies (e.g.

460 Zaaijer, 2006; Sørensen and Ibsen, 2013). This feature is likely due to the mode shape for this mode, in
461 which relatively large amplitudes occur at bed level. For working wind turbine support structures,
462 measurements of the second natural frequency are likely to provide a particularly sensitive indication of the
463 presence of scour.

464 The scour-only tests confirm that scour processes invariably cause significant reductions in the stiffness
465 of the foundation (as indicated by the lowering of the natural frequencies). Two distinct mechanisms are
466 considered to occur; (A) scour processes remove soil that would otherwise contribute lateral stiffness to the
467 pile hence increasing the free length; and (B) scour processes reduce the effective stresses in the remaining
468 soil adjacent to the pile due to loss of overburden. Since the stiffness (small strain shear modulus) of the
469 sand is known to depend on the magnitude of the *in situ* stresses, the loss of overburden in Mechanism B
470 causes the stiffness of the soil adjacent to the pile to reduce. Scour protection systems (when present) are
471 considered to modify the dynamic characteristics of the system by reversing these two detrimental
472 mechanisms. Effective reversal of Mechanism A requires that scour protection systems are stiff and well-
473 compacted against the monopile. The reversal of Mechanism B relies only on the surcharge applied by the
474 scour protection material.

475 The installation of remedial rock fill scour protection was found to increase the natural frequencies,
476 although the magnitude of the effect was variable. In all cases the installation of rock fill did not restore the
477 natural frequencies to values corresponding to an equivalent additional pile embedment in undisturbed sand.
478 Although it can be confidently assumed that the additional surcharge provided by the rock will have
479 contributed to additional foundation stiffness via the reversal of Mechanism B, the effectiveness of the direct
480 stiffness contribution (reversal of Mechanism A) is in this case uncertain. It is considered likely that the direct
481 stiffness contribution is relatively modest in the current experiments since – following normal practice in the
482 field – no attempt was made to compact the rock against the pile. A smaller diameter rock (d_{50}/D ~ 0.05)
483 with high density may be beneficial for Mechanism B (not explored in these tests).

484 There was an observed tendency in some cases for the natural frequencies to increase slightly after the
485 rock fill material had been placed and further flow cycles had been conducted. It is considered that this effect
486 is a consequence of the sand accretion within the rock material that was invariably observed at the end of
487 each test. This accreted sand is likely to have (i) slightly increased the local surcharge and (ii) developed a
488 stiffer interface between the rock material and the pile by the filling of voids. Sand accretion in rock berms
489 has previously been observed in the laboratory by An et al. (2014) but it is believed that the current tests

provide the first published observation of this mechanism in connection with scour protection systems for monopile foundations. The role of suction scour has been assessed in the current tests on the basis of the results of An et al. (2014, Figure 5) which delimits when suction is in operation. The sediment ratio d_{50}(sand)/d_{50}(rock) = 0.161 mm/18.3 mm = 8.8 10^{-3} and the bed mobility θ is estimated at 0.33 for the global scour phase of the current tests. When plotted on the diagram of An et al. we are in the 'no motion' region of the diagram and hence suction scour is ruled out.

The effectiveness of the remedial rock fill scour protection configuration, in terms of the influence of further global scouring, depended on the installed thickness. For thin layers of limited extent, subsequent global scouring caused substantial further reductions in the observed natural frequencies. This is considered to be associated with the 'falling apron' mechanism that was observed in the tests. More substantial rock fill layers with further recovery of the foundation stiffness (presumably due to the additional effects of sand accretion) also had the potential for reductions in natural frequency during subsequent global scouring.

Tyre-filled net remedial scour protection was shown to provide relatively small increases in both foundation stiffness and subsequent recovery with sand accretion. It appears that the relatively lightweight low stiffness nature of this system does not reverse Mechanisms A and B in any significant way. However, the tyre-filled nets were shown to be successful in achieving a stable local bed level, thereby maintaining the dynamic characteristics of the structure against further erosion.

Pre-installed rock armour scour protection was shown to provide significant protection from local and global scouring. Some increase in the natural frequency of the structure was observed, attributed to sand accretion within the rock matrix during flow cycles.

CONCLUSIONS

Analysis of the structural dynamics of a scaled wind turbine monopile-tower system exposed to local and global scour, and scour remediation, in large-scale laboratory tests has demonstrated the changes that can occur in the first three natural frequencies. The mode 1 frequency is especially sensitive to tower top mass and the mode 2 frequency is most sensitive to scour effects.

The results of this study inform the site by site assessment and modelling of scour effects and their impact on structural performance. The main conclusions are:

(1) Pre-installed scour protection systems have the principal purpose of preventing local erosion around the monopile. Pre-installed rock – intended to mimic typical systems employed in practice – was shown to provide effective protection in the current tests.

(2) Remedial scour protection systems typically have the dual purpose of preventing further erosion and restoring the dynamic characteristics of the system to acceptable levels. The current experiments demonstrate that the effectiveness of remedial scour protection systems in controlling further erosion is variable. Relatively thick rock fill layers are shown to be effective; tyre-filled nets also demonstrated a significant erosion control capability. None of the remedial configurations that were tested, however, provided a wholly effective means of restoring the system dynamics. The rock fill material provided some stiffness recovery, but the rock appears to have been deposited in a loose state with the consequence that the stiffness of the deposited material is lower than that of the *in situ* sand. The stiffness contribution of tyre-filled nets was observed to be low.

(3) The test results imply the following tentative conclusions for full-scale structures:

(i) Employing pre-installed scour protection is likely to be a more effective way of controlling scour processes than by managing the erosion via post-construction remedial scour protection measures.

(ii) Tyre-filled nets provide an effective means of slowing the erosion processes although they are otherwise ineffective in improving the system dynamics.

(iii) Rock fill remedial scour protection is effective in both arresting further scour and adding stiffness to the system, although a sufficiently large volume of material needs to be installed for these two actions to be effective. The benefit of installing high density rock (not tested) in adding stiffness to the system could be considered.

(iv) Sand accretion within the scour protection systems can provide a useful enhancement of performance in terms of system dynamics. However, with no known published excavations of offshore scour protection systems known to the authors, it is unclear to what extent this sand accretion would occur in the field and therefore what potential stiffness increases might be expected. There may be scope to specify the grading of scour protection systems to maximise the effectiveness of the sand accretion mechanism.

ACKNOWLEDGEMENTS

This research project is supported through funding from E.On Climate and Renewables (recently renamed to RWE Renewables) and HR Wallingford, and by grant EP/L016303/1 for Cranfield University, the University of Oxford and Strathclyde University, Centre for Doctoral Training in Renewable Energy Marine

Structures - REMS (http://www.rems-cdt.ac.uk/) from the UK Engineering and Physical Sciences Research Council (EPSRC). Byrne is supported by the Royal Academy of Engineering under the Research Chairs and Senior Research Fellowships scheme.

The Authors gratefully acknowledge the work of team members at HR Wallingford, E.On and Oxford University, who aided in the implementation and execution of the testing program. In addition, the Authors gratefully acknowledge Fugro for triaxial testing performed as input to the soil characterisation for the experiments.

DATA AVAILABILITY

The following data are available on request from ross.mcadam@eng.ox.ac.uk: detail of model monopile – tower system, soil characterisation results, bathymetry results, natural frequency results.

NOTATION LIST

The following symbols are used in this paper:

A = Cross-sectional area;

b = Scour protection width;

B = Small strain shear modulus coefficient;

d_{xx} = Sand particle diameter coefficient (xx^{th} percentile);

D = Pile diameter;

D_R = Sand relative density;

e = Soil voids ratio;

E = Young's modulus;

EI = Flexural stiffness;

$f_{n,m}$ = Natural frequency for mode m;

G_0 = Soil small strain shear modulus;

G_S = Soil specific gravity;

h_w = Water depth;

H_B = Depth of sand below pile tip;

L = Pile embedment length;

L_X = Geometric length (of structure component X);

M = Bending moment;

M_{Top} = Structure top mass;

n = Soil porosity;

N_{cyc} = Number of flow cycles;

N_M = Number of top masses;

p' = Mean effective stress;

p_{ref} = Reference stress;

q_c = CPT bearing stress;

r = Radial distance from pile centerline;

S_G = Global scour bathymetry reduction;

S_L = Local scour bathymetry reduction;

S_T = Total scour bathymetry reduction;

t_w = Pile wall thickness;

t_{sp} = Scour protection thickness adjacent to the pile wall;

T_f = Elapsed flow time;

$\overline{U}$ = Depth averaged flow velocity;

v = Displacement;

x = Coordinate in the streamwise direction;

y = Coordinate in the spanwise direction;

z = Distance above pile toe;

γ = Soil unit weight;

$\omega_{n,m}$ = Circular natural frequency for mode m;

ζ_m = Damping ratio for mode m;

ϕ_m = Phase angle for mode m;

ρ = Material density;

ρ_w = Water density, assumed 1000 kg.m^{-3};

σ_v' = Soil effective vertical stress;

ν = Kinematic viscosity of water;

609 **REFERENCES**

610 Abadie, C.N., Byrne, B.W. and Levy-Paing, S. (2015). “Model pile response to multi-amplitude cyclic lateral
611 loading in cohesionless soils”. In: International Symposium on Frontiers in Offshore Geotechnics, 2015-6-
612 10 to 2015-6-12, ISFOG, Oslo, Norway pp. 681-686.

613 An, H., Cheng, L., Luo, L., Draper, S., White, D. and Jas, E. (2014). “Effect of sediment supply on suction
614 scour under a rock berm”. In Proceedings of the 7th International Conference on Scour and Erosion,
615 ICSE 2014. vol. 1, Taylor & Francis, London, UK, pp. 265 - 273, 7th International Conference on Scour
616 and Erosion, Perth, Australia, 2/12/14.

617 API (2011). RP 2GEO - Recommended Practice for Geotechnical Foundation Design Consideration.
618 Washington: American Petroleum Institute.

619 Arany, L., Bhattacharya, S., Macdonald, J.H. and Hogan, S.J. (2016). “Closed form solution of Eigen
620 frequency of monopile supported offshore wind turbines in deeper waters incorporating stiffness of
621 substructure and SSI”. Soil Dynamics and Earthquake Engineering, 83, pp.18-32.

622 Arboleda Chavez, C., Stratigaki, V., Wu, M., Troch, P., Schendel, A., Welzel, M., Villanueva, R., Schlurmann,
623 T., De Vos, L., Kisacik, D., Taveira Pinto, F., Ferradosa, T., Santos, P.R., Baelus, L., Szengel, V., Bolle,
624 A., Whitehouse, R. and Todd, D. (2019). “Large scale experiments to improve monopile scour protection
625 design adapted to climate change – The PROTEUS project.” Energies 2019, 12(9), 1709;
626 https://doi.org/10.3390/en12091709

627 Baldi, G., Bellotti, R., Ghionna, V.N., Jamiolkowski, M. and Lo Presti, D.C.F., (1989), August. Modulus of
628 sands from CPTs and DMTs. In Proc. 12th ICSMFE (Vol. 1, pp. 165-170).

629 Burd, H.J., Taborda, D.M.G. Zdravković, L. Abadie, C.N., Byrne, B.W., Houlsby, G.T., Gavin, K.G., Igoe,
630 D.J.P., Jardine, R.J., Martin, C.M., McAdam, R.A., Pedro, A.M.G., and Potts, D.M. (2019). PISA Design
631 Model for Monopiles for Offshore Wind Turbines: Application to a Marine Sand. Geotechnique
632 doi.org/10.1680/jgeot.18.P.277

633 Craig, R.F. (1992). Craig's Soil Mechanics. London, Spon Press.

634 De Vos, L., De Rouck, J., Troch, P. and Frigaard, P. (2011). “Empirical design of scour protections around
635 monopile foundations Part 1: Static approach”. Coastal Engineering 58 540-553.

636 DNVGL (2016). Standard DNVGL-ST-0126, Support structures for wind turbines, Edition April 2016.

637 Hardin, B.O., and Richart Jr, F.E. (1963). “Elastic wave velocities in granular soils”. Journal of Soil
638 Mechanics & Foundations Div, 89 (Proc. Paper 3407).

639 Hucker, N., Ward, I. and Manceau, S. (2019). “Measured changes in the natural frequency of offshore wind
640 turbines with monopile foundations”. Proceedings SECED 2019 Conference, 9-10 September 2019,
641 Greenwich, London.
642 Jamiolkowski, M., Ladd, C.C., Germaine, J.T. and Lancelotta, R. (1985). “New developments in field and
643 laboratory testing of soils. State-of-the-art report”. Proceedings of the 11th International Conference on
644 Soil Mechanics and Foundation Engineering, San Francisco, 1, 57-153, Balkema Pub., Rotterdam.
645 Jardine, R.J., Chow, F.C., Overy, R. and Standing, J. R. (2005). “ICP design methods for driven piles in
646 sands and clays”. Thomas Telford Ltd, London, p 105.
647 Mayall, R.O., Byrne, B.W., Burd, H.J., McAdam, R.A., Cassie, P. and Whitehouse, R.J.S. (2019), "Modelling
648 of foundation response to scour and scour protection for offshore wind turbine structures", Scour and
649 Erosion IX - Proceedings of the 9th International Conference on Scour and Erosion, ICSE 2018, pp. 405.
650 Mayall, R.O., McAdam, R.A., Byrne, B.W., Burd, H.J., Sheil, B.B., Cassie, P. and Whitehouse, R.J.S. (2018),
651 "Experimental modelling of the effects of scour on offshore wind turbine monopile foundations", Physical
652 Modelling in Geotechnics, pp. 725.
653 Petersen, T.U., Nielsen, A.W., Hansen, D.A., Pedersen, A.V., Christensen, E.D. and Fredsøe, J. (2019).
654 “Stability of single-graded scour protection around a monopile in current”. Scour and Erosion IX -
655 Proceedings of the 9th International Conference on Scour and Erosion, ICSE 2018, pp. 405.
656 Poulos, H. G. and Davis, E. H. (1980). Pile foundation analysis and design, John Wiley & Sons, New York.
657 Prendergast, L.J., Hester, D., Gavin, K. and O'Sullivan, J.J. (2013). "An investigation of the changes in the
658 natural frequency of a pile affected by scour", Journal of Sound and Vibration, vol. 332, no. 25, pp. 6685-
659 6702.
660 Prendergast, L.J., Gavin, K. and Doherty, P. (2015). "An investigation into the effect of scour on the natural
661 frequency of an offshore wind turbine", Ocean Engineering, vol. 101, pp. 1-11.
662 Qi, W.G., Gao, F.P., Randolph, M.F. and Lehane, B.M. (2016). "Scour effects on p–y curves for shallowly
663 embedded piles in sand", Geotechnique, vol. 66, no. 8, pp. 648-660.
664 Riezebos, H., Raaijmakers, T., Tönnies-Lohmann, A.,Waßmuth, S. and Van Steijn, P. (2016). “Scour
665 protection design in highly morphodynamic environments”. In: ICSE 2016 (8th International Conference
666 on Scour and Erosion), 12-15 September 2016, Oxford, UK. (2016)
667 Rix, G.J. and Stokoe, K.H. (1991), "Correlation of initial tangent modulus and cone penetration resistance",
668 Huang, A.B. (Ed.), Calibration Chamber Testing: Proceedings of the First International Symposium on

669 Calibration Chamber Testing ISOCCTI, Potsdam, New York, 28-29 June 1991, Elsevier Science
670 Publishing Company, New York, pp. 351-362.
671 Sørensen, S.P.H. and Ibsen, L.B. (2013). "Assessment of foundation design for offshore monopiles
672 unprotected against scour". Ocean Engineering 63 17-25.
673 Soulsby, R.L. (1997). Dynamics of marine sands, London: Thomas Telford.
674 Sumer, B.M, Christiansen, N. and Fredsøe, J. (1992). "Time scale of scour around a vertical pile". In: Proc.
675 2nd Int. Offshore and Polar Eng. Conf., ISOPE, San Francisco, USA, Vol. 3, pp. 308 – 315.
676 Whitehouse, R.J.S. (1998). Scour at marine structures, London. Thomas Telford.
677 Whitehouse, R.J.S., Harris, J.M., Sutherland, J. and Rees, J. (2011). "The nature of scour development and
678 scour protection at offshore windfarm foundation". Marine Pollution Bulletin 62 73-88.
679 Whitehouse, R., Sutherland, J., Powell, K. and Harris, J. (2014). "Fast flow facility for sediment and
680 morphology testing". In: Coastlab 14, 29 September – 2 October 2014, Varna, Bulgaria (eds. V. Penchev
681 and F.T. Pinto), pp 104-113.
682 Zaaijer, M. B. (2006). "Foundation modelling to assess dynamic behaviour of offshore wind turbines". Applied
683 Ocean Research, 28, 45–57.
684

685 **TABLES**

686 **Table 1.** Properties of Bathgate sand

d_{10} (mm)	d_{50} (mm)	d_{90} (mm)	G_s	e_{min}	e_{max}
0.077	0.161	0.282	2.65	0.502	0.753

687

688 **Table 2.** Pile and tower geometry and properties

Component	Material	Length (m)	Outer diameter D (m)	Wall thickness t_w (mm)	Longitudinal modulus E (GPa)	Density ρ (kg/m^3)
Monopile	GFRP	2.5	0.197	3.5	31.235	1855
Tower	Aluminium	3.2	0.1016	1.6	69	2700

689

690 **Table 3.** Monopile-tower structure dimensionless groups at full scale and experiment scale

Dimensionless group		Robin Rigg[a]	Arany et al. (2016) dataset	Experiment design
Pile slenderness	L/D	4.6 – 6.3	4.3 – 9.4	4.5 – 5.5
Pile wall thickness	D/t_w	57 – 96	50 – 106	56
Tower height	L_t/L_{pile}	1.09 – 1.24	0.74 – 1.73	1.2
Pile relative stiffness (Poulos & Davis, 1980; Abadie et al., 2015)	E_pI_p/E_sL^4	8E-4 – 5E-3	(not assessed)	2E-3 – 5E-3
Tower relative stiffness (Arany et al., 2016)	E_tI_t/E_pI_p	0.11 – 0.18	0.12 – 0.71	0.15
Mass ratio (Arany et al., 2016)	M_{Top}/M_t	1.0	0.5 – 1.3	0.04 – 1.6 (0.83 for N_M = 3)

Where: L_t is the tower length excluding the transition piece, E_pI_p is the flexural stiffness of the monopile, E_s is a reference soil stiffness estimated at the pile tip using the relationship $E_s = 2(1+\nu)G_0$ where ν is the Poission's ratio (assumed as 0.5) and G_0 is the small strain shear modulus calculated using Equation (2), E_tI_t is the average flexural stiffness of the tower, M_{Top} is the mass attached to the top of the tower, M_t is the mass of the tower excluding attachments

[a] Robin Rigg offshore wind farm data supplied by E.On Energy

691

692 **Table 4.** Mass and location of pile/tower assembly peripherals

Component	Height of centre of gravity above pile tip z (m)	Mass (kg)
Transition piece	2.38	2.83
Accelerometers and mounting	2.33, 2.83, 3.18, 3.53, 4.13, 5.38	0.07 (per height)
Force sensors and mounting	5.47	0.30
Top masses (N_M = 1)	5.49	1.11
Top masses (N_M = 3)	5.51	3.32
Top masses (N_M = 6)	5.54	6.64

693

694 **Table 5.** Test matrix and target scour depths

Test	Initial condition		Local scour phase		Global scour phase		
	Target pile embedment L/D	Target water depth h_w/D	Target local scour S_L/D	Target global scour S_L/D	Scour protection system		Target global scour S_G/D
1	4.5	4.5	1.5	0	None		1.5
2	4.5	4.5	1.5	0	Tyre-filled nets (remedial)	(R-TFN)	1.5
3	4.5	4.5	1.5	0	Rock fill (remedial)	(R-RF1)	1.5
4	4.5	4.5	0.75	0	Rock fill in partial scour hole (remedial)	(R-RF2)	1.5
5	4.5	4.5	0.0	0	Pre-installed rock armour	(P-RA)	1.5
6	5.5	3.5	1.5	0	Rock fill (remedial)	(R-RF3)	2.5

695

696 **Table 6.** Small strain shear modulus tests

Test ID	Test Type	e	D_R [%]
BE1_Loose	Bender Element	0.665	35.1
BE2_Medium	Bender Element	0.599	61.3
BE3_Dense	Bender Element	0.531	88.5
RC1_Medium	Resonant Column	0.582	68.0

697

698

699 **Table 7.** Pile embedded lengths and plug lengths

Test	Installed embedded length L/D	Plug length z_{plug}/D
1	4.56	4.04
2	4.61	4.29
3	4.57	4.43
4	4.55	4.33
5	4.57	4.37
6	5.61	5.33

700

701 **Table 8.** Definition of flow regimes for scouring phases. N_{cyc} is the total number of symmetrical flow cycles
702 employed

Phase	1a	1b	2a	2b	2c	2d[e]	2e[e]
$\overline{U}$ (m/s)	0.35[a]	0.55[b]	0.70	0.70	0.70	0.70	0.70
Flow time (mins)	166	332[c]	498	498	498	498	498
N_{cyc}	1	2[c]	3	2[d]	2	2	2
Scour type	Local	Local	Global	Global	Global	Global	Global
Target $\Delta S/D$	0.75	0.75	0.5	0.5	0.5	0.5	0.5

Exceptions:

[a] Test 1, Phase 1a: $\overline{U}$ = 0.40 m/s

[b] Test 6, Phase 1b: $\overline{U}$ = 0.50 m/s

[c] Test 4, Phase 1b: Flow time = 0, N_{cyc} = 0

[d] Test 3, Phase 2b: N_{cyc} = 3 repeating Phase 2a

[e] Phase 2d and 2e: Only used for Test 6, with a 3:1 asymmetry in the duration of forward flow to transport more sediment from test bed

703

704

705 **Table 9.** Overview of achieved scour depths

Test	After local scour development (End of flow Phase 1)		After global scour development (End of flow Phase 2)
	Total scour S_T/D	Global scour S_G/D	Global scour S_G/D
1	1.58	0.14	0.57
2 (TFN)	1.58	0.09	0.43
3 (R-RF1)	1.49	0.21	0.30
4 (R-RF2)	0.66	-0.02	0.36
5 (P-RA)	-	0.14	0.46
6 (R-RF3)	1.51	0.15	1.79

706

707 **Table 10.** In-place scour protection system characteristics

Test		Installed height at pile wall t_{sp}/D	Width b/D	Bulk unit weight γ (kN/m^3)	Bulk voids ratio e	Bulk porosity n
2 (R-TFN)	Tyre-filled nets	1.23	0.7	10.14	4.960	0.832
3 (R-RF1)	Rock fill	0.82	2.2	18.85	0.953	0.488
4 (R-RF2)	Rock fill in partial scour hole	0.54	1.1	18.99	0.923	0.480
5 (P-RA)	Preinstalled rock	0.28[a]	3.2	18.04	1.146	0.534
6 (R-RF3)	Rock fill	1.02	1.7	18.60	1.008	0.502

708 Note: [a] this is the measured thickness at the pile wall once the protective collar had been removed after pile
709 driving analysed according to Fig. 7(b).

710

711 **FIGURES**

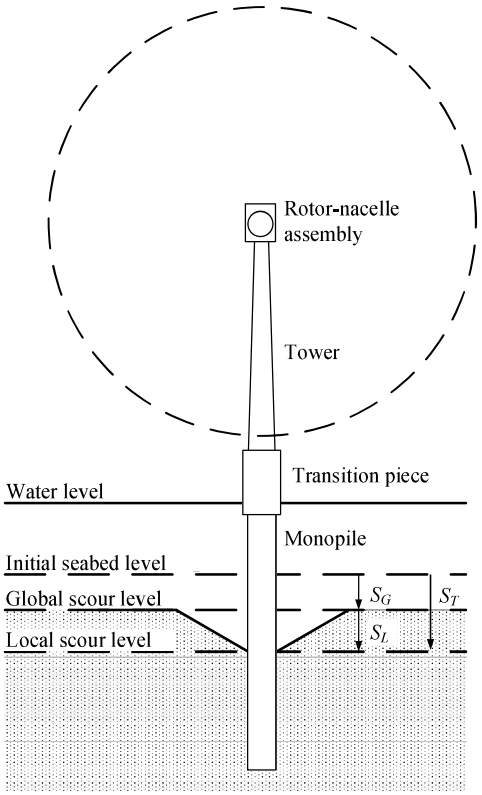

Fig. 1. Idealised seabed profile due to local and global scour (after Mayall et al., 2018)

712

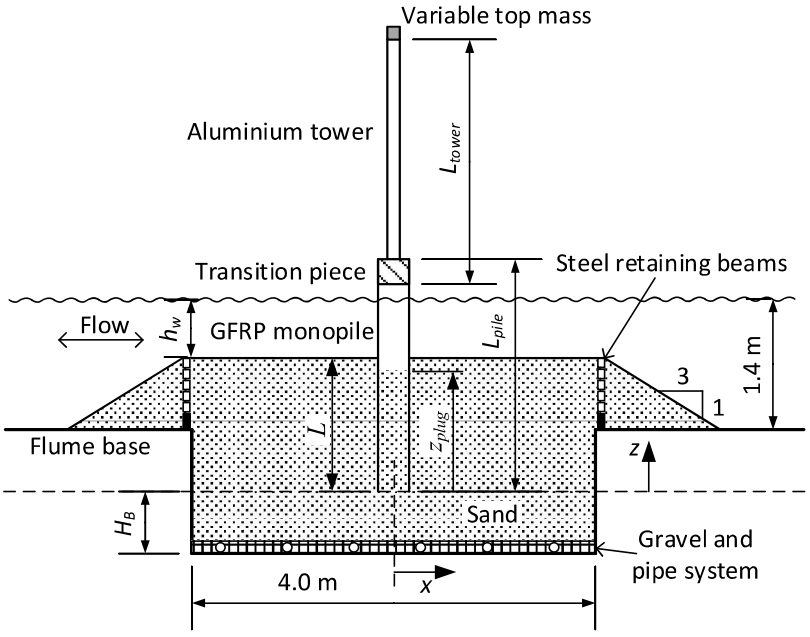

Fig. 2. Annotated section view of the prepared sand bed and monopile - tower system (not to scale)

713

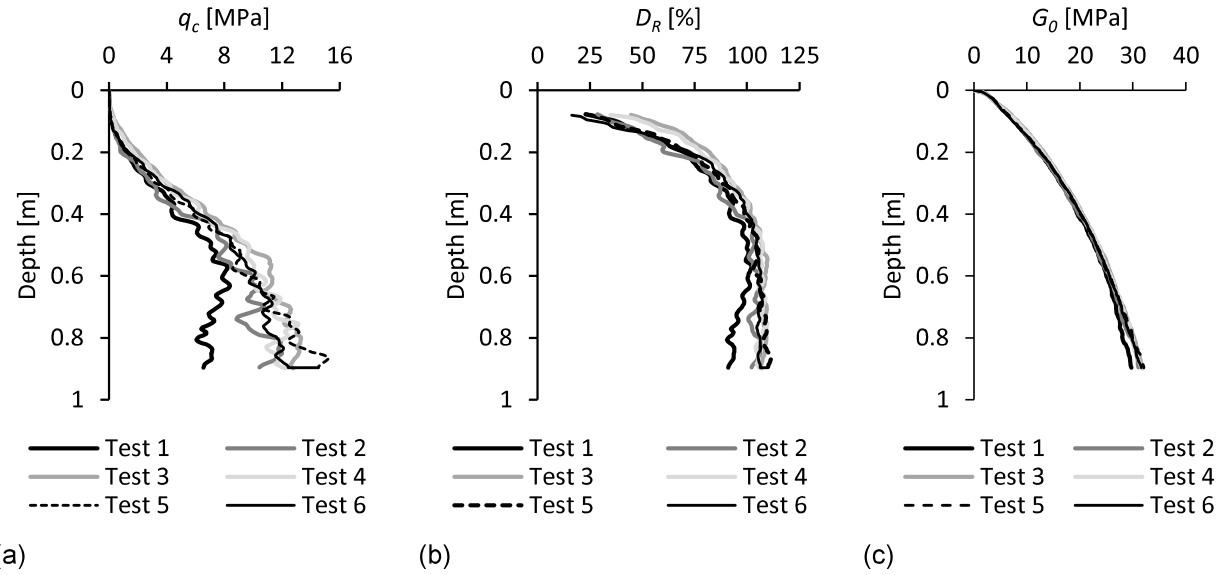

Fig. 3. Test bed CPT measurements on (a) end bearing, q_c; (b) inferred relative density D_R; (c) inferred small strain shear modulus, G_0

714

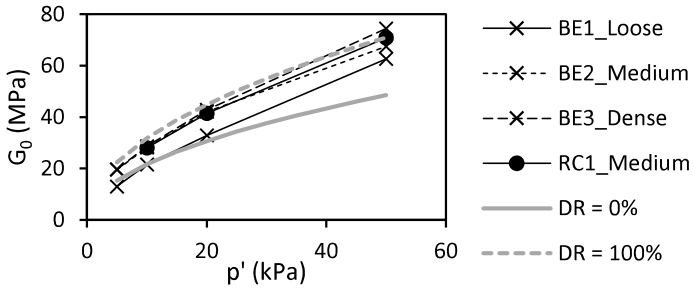

Fig. 4. Measured small strain shear modulus, G_0. Also shown is the correlation in Equation (2) with $B = 478$ for $D_R = 0$ and 100%

715

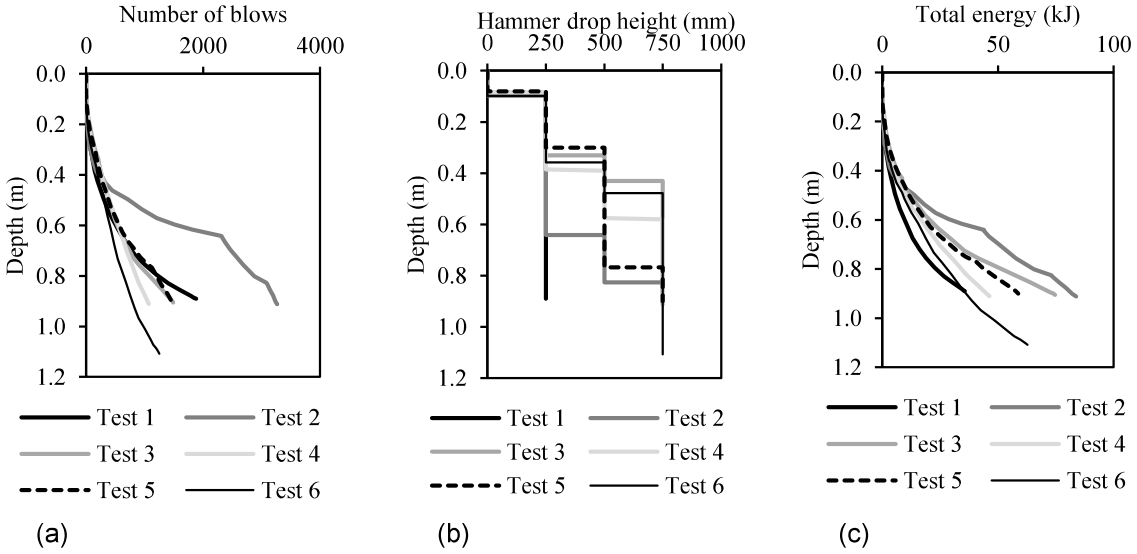

Fig. 5. Driving records (a) Driving number of blows; (b) Hammer drop height; (c) Driving energy

716

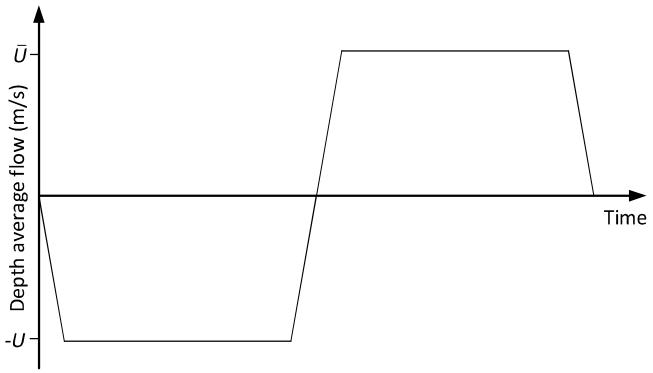

Fig. 6. Illustration of a typical symmetrical flow cycle

717

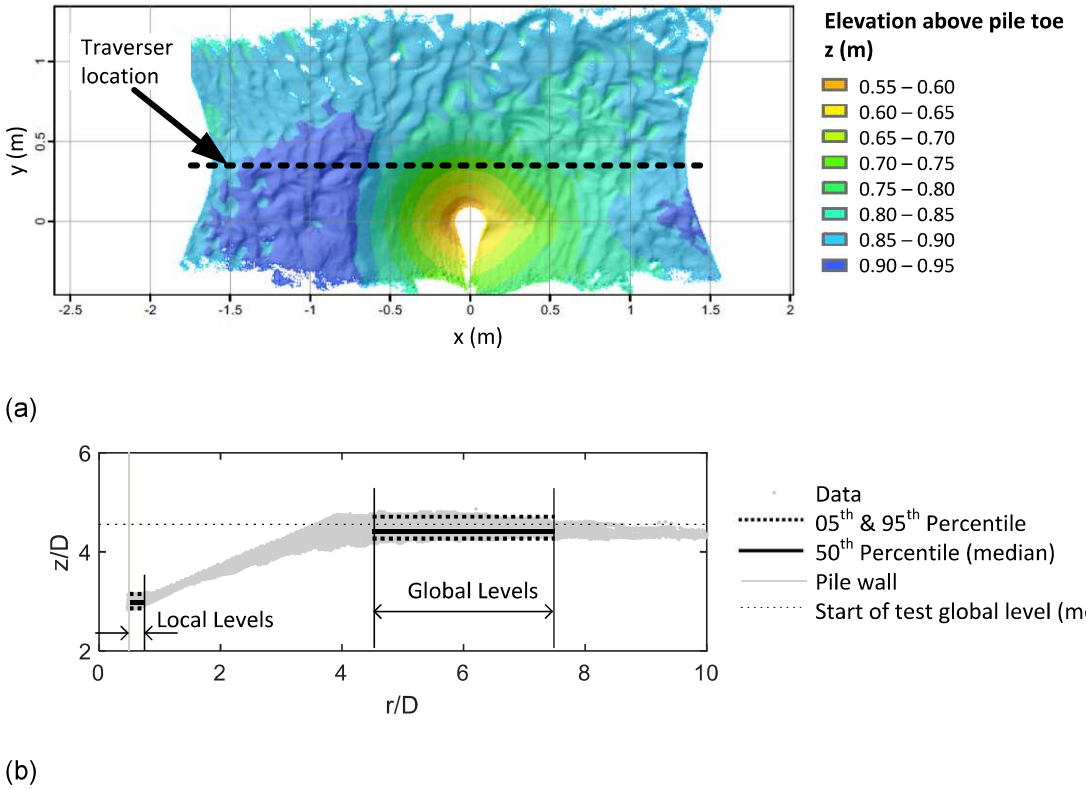

Fig. 7. Typical profile of scour (Test 1, end of flow Phase 1b) (a) Plan bathymetry plot with hillshade to highlight detail, indicating the underwater laser scanner traverser location; (b) Bathymetry section interpretation, individual data points appear as a grey band

718

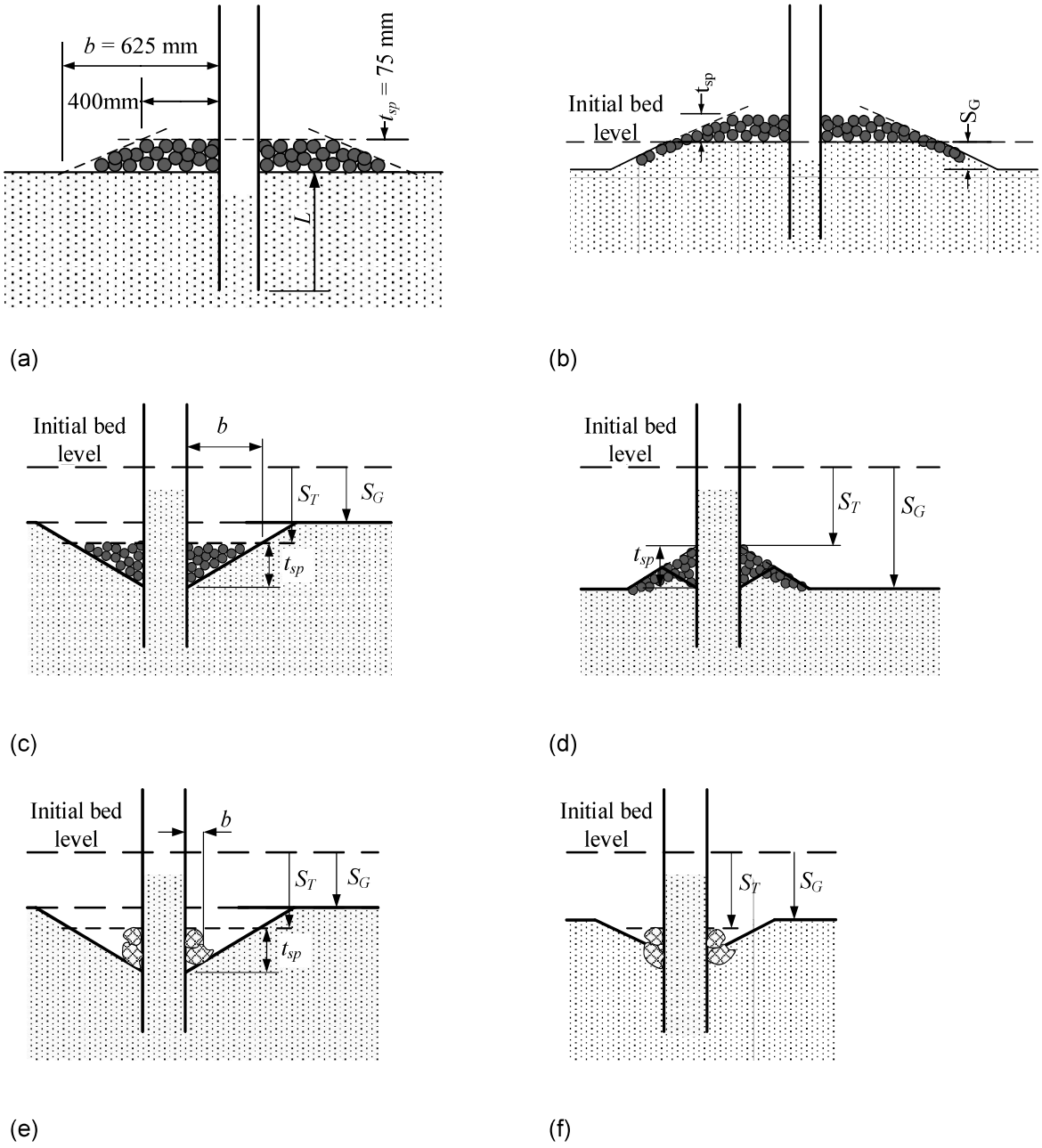

Fig. 8. Geometric definitions for scour protection systems (a) Preinstalled rock armour (Test 5); (b) Pre-installed rock armour following global scour; (c) Rock fill in scour hole (Tests 3, 4 & 6); (d) Rock fill following global scour; (e) Tyre-filled nets (Test 2); (f) Tyre-filled nets following global scour

719

(a) (b) (c)

Fig. 9. Photographs of installed scour protection systems; (a) Tyre-filled nets (Test 2); (b) Rock fill (Tests 3, 4, 6); (c) Pre-installed rock (Test 5)

720

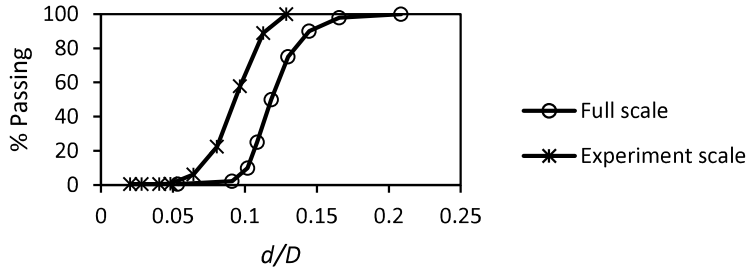

Fig. 10. Dimensionless rock scour protection grading curves at full scale and experiment scale

721

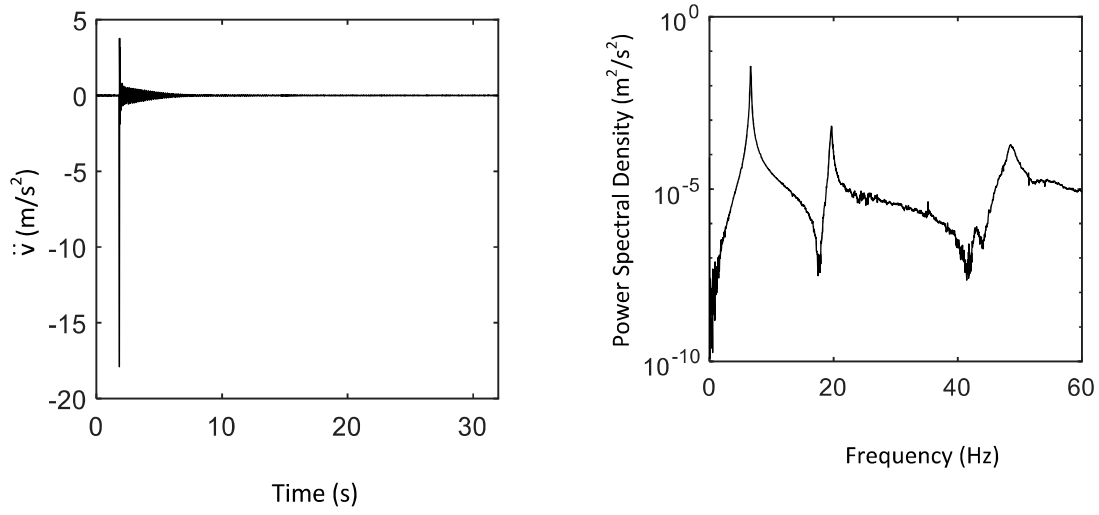

(a) (b)

Fig. 11. Example signal and power spectral density (start of Test 3, N_M = 0, top accelerometer, streamwise); (a) Recorded acceleration; (b) Power spectral density

722

723

724

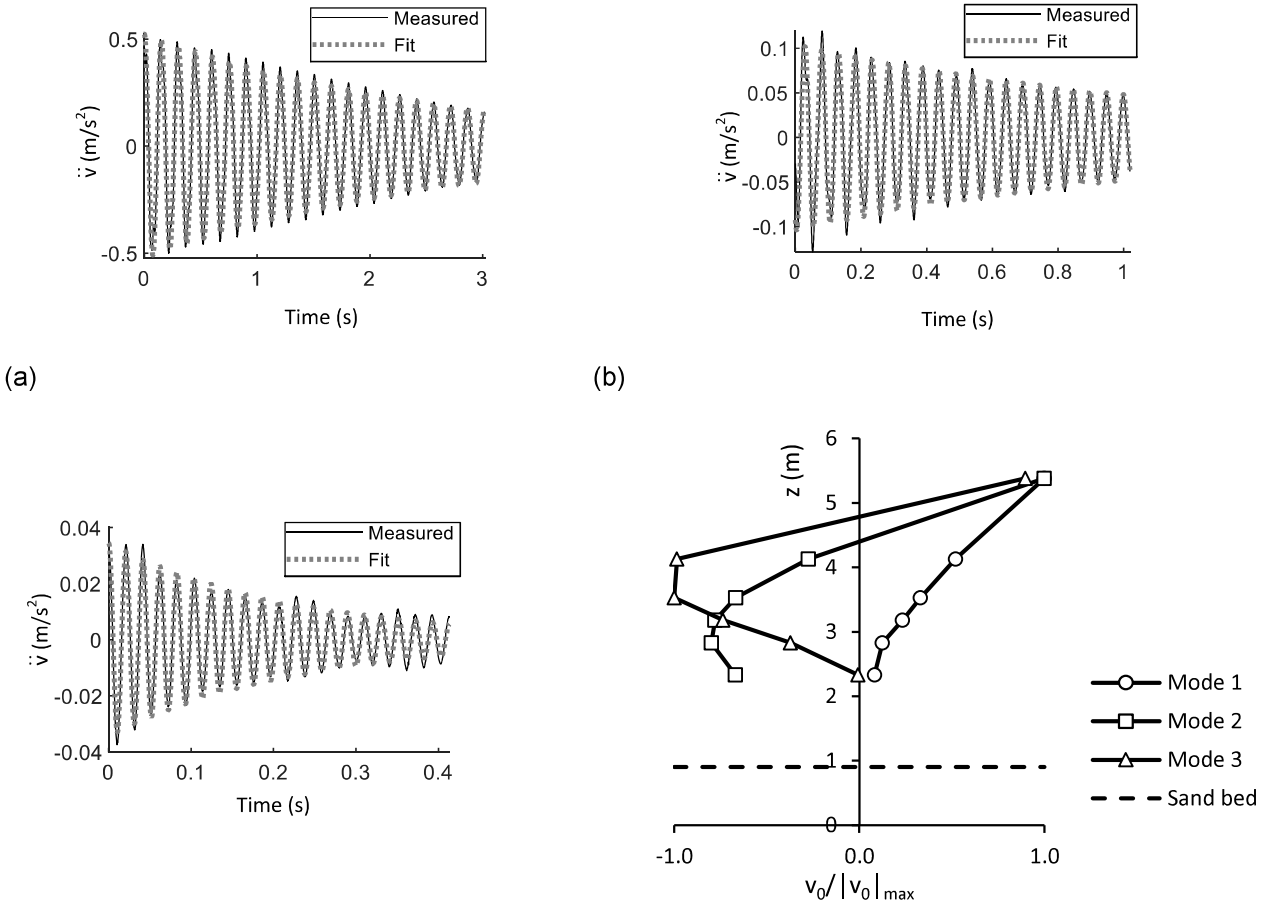

Fig. 12. Example calculation of natural frequencies (start of Test 3, N_M = 0, top accelerometer, streamwise). Also shown are the mode shapes. (a) First mode measured signal fitting (f_n = 6.63 Hz, ζ = 0.9 %); (b) Second mode residual signal fitting (f_n = 19.6 Hz, ζ = 0.6 %); (c) Third mode residual signal fitting (f_n = 48.4 Hz, ζ = 1.4 %); (d) Mode shapes with height above pile tip – initial sand bed at z = 0.9 m

725

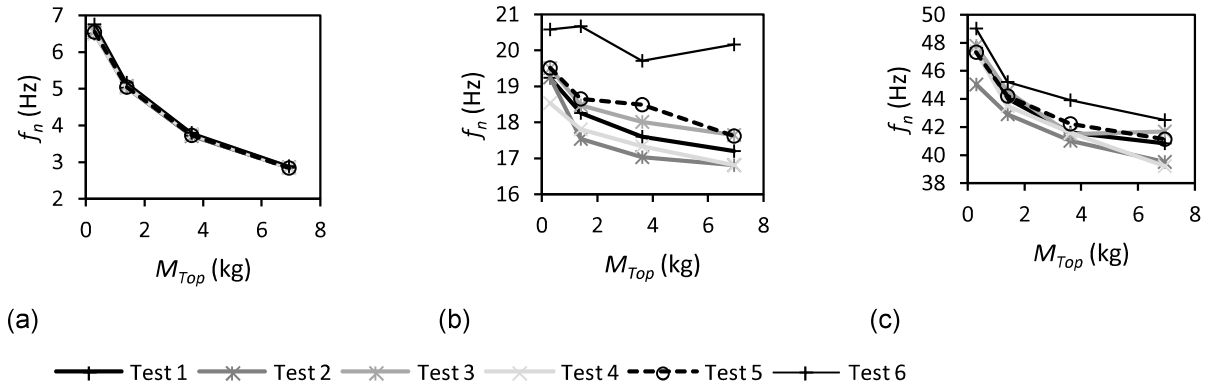

Fig. 13. Influence of top mass on the inferred natural frequency at the start of each test; (a) Mode 1 natural frequency; (b) Mode 2 natural frequency; (c) Mode 3 natural frequency

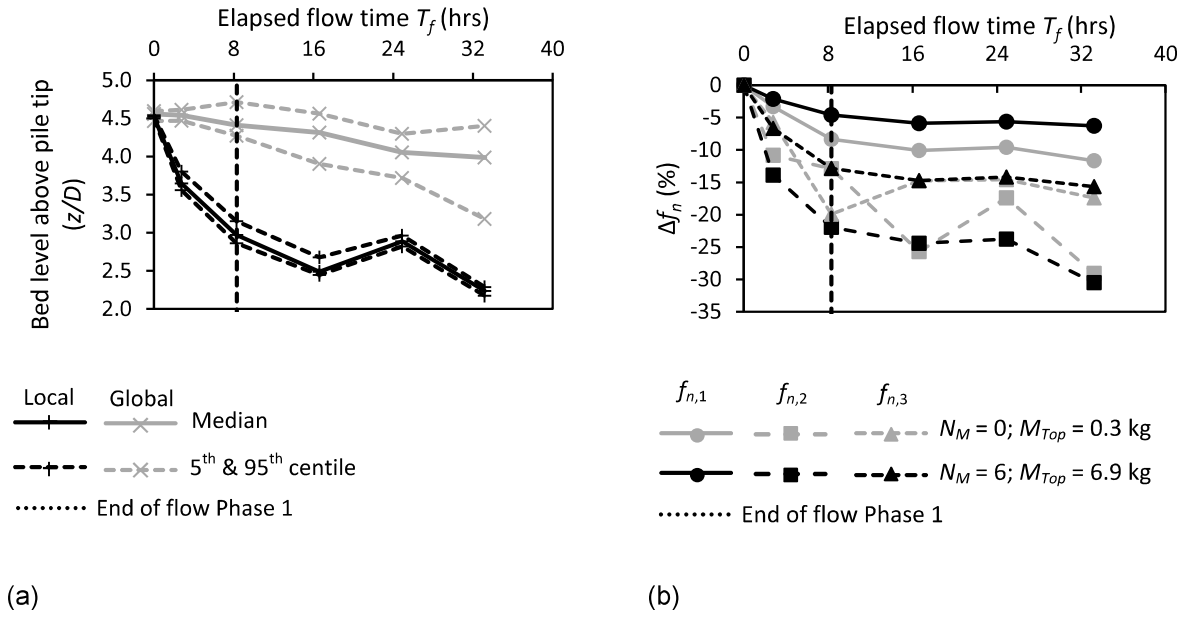

Fig. 14. Experiment results – measured bathymetry and inferred natural frequencies for experiment with unremediated scour (Test 1); (a) Bathymetry outputs; (b) Change in natural frequency

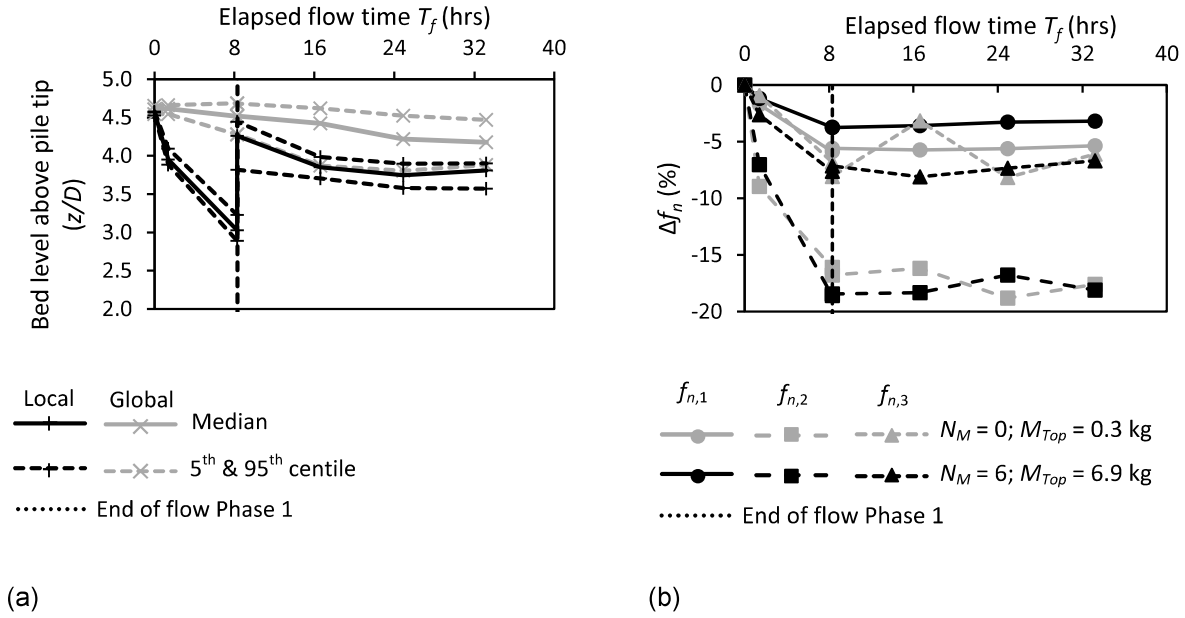

Fig. 15. Experiment results – Tyre-filled net remedial scour protection (Test 2); (a) Bathymetry outputs; (b) Change in natural frequency

730

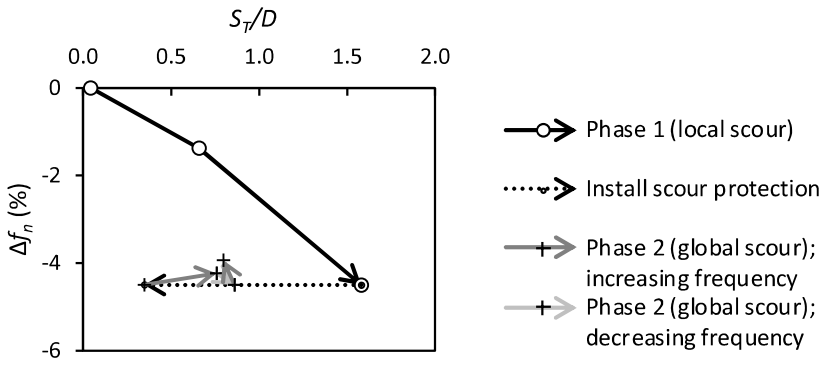

Fig. 16. Mean relative change in mode 1 natural frequency (for N_M = 0, 1, 3, 6) with tyre-filled net remedial scour protection (Test 2)

731

(a) (b)

Fig. 17. Photographs of tyre-filled net remedial scour protection after all flow phases, arrows approximately indicate the flume x-axis direction (see Fig. 2); (a) After draining flume; (b) After removing top layer of tyre-filled nets

732

733

734

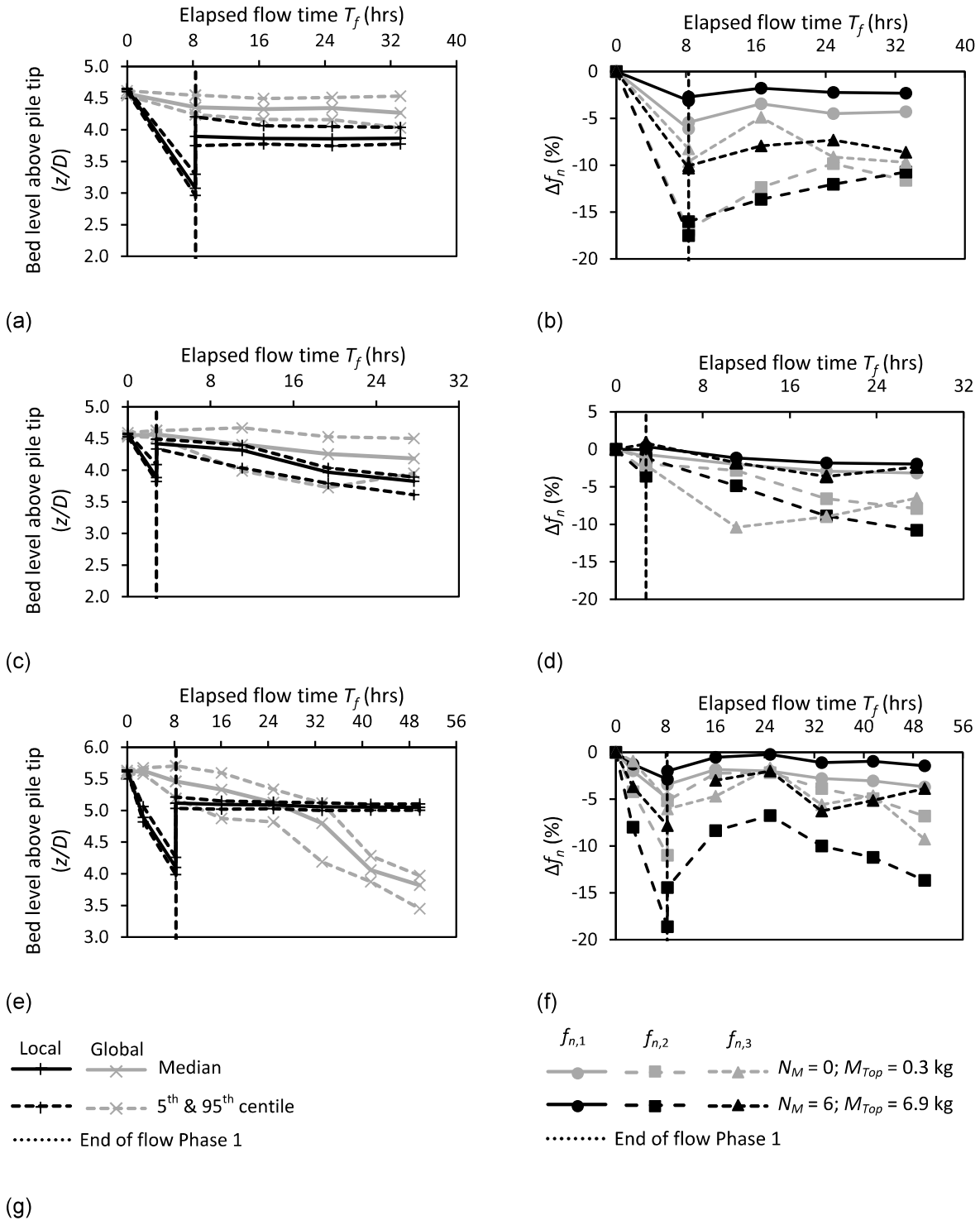

Fig. 18. Experiment results – Rock fill remedial scour protection (Test 3, 4 and 6); (a) Bathymetry outputs (Test 3); (b) Change in natural frequency (Test 3); (c) Bathymetry outputs (Test 4); (d) Change in natural frequency (Test 4); (e) Bathymetry outputs (Test 6); (f) Change in natural frequency (Test 6); (g) Legends

735

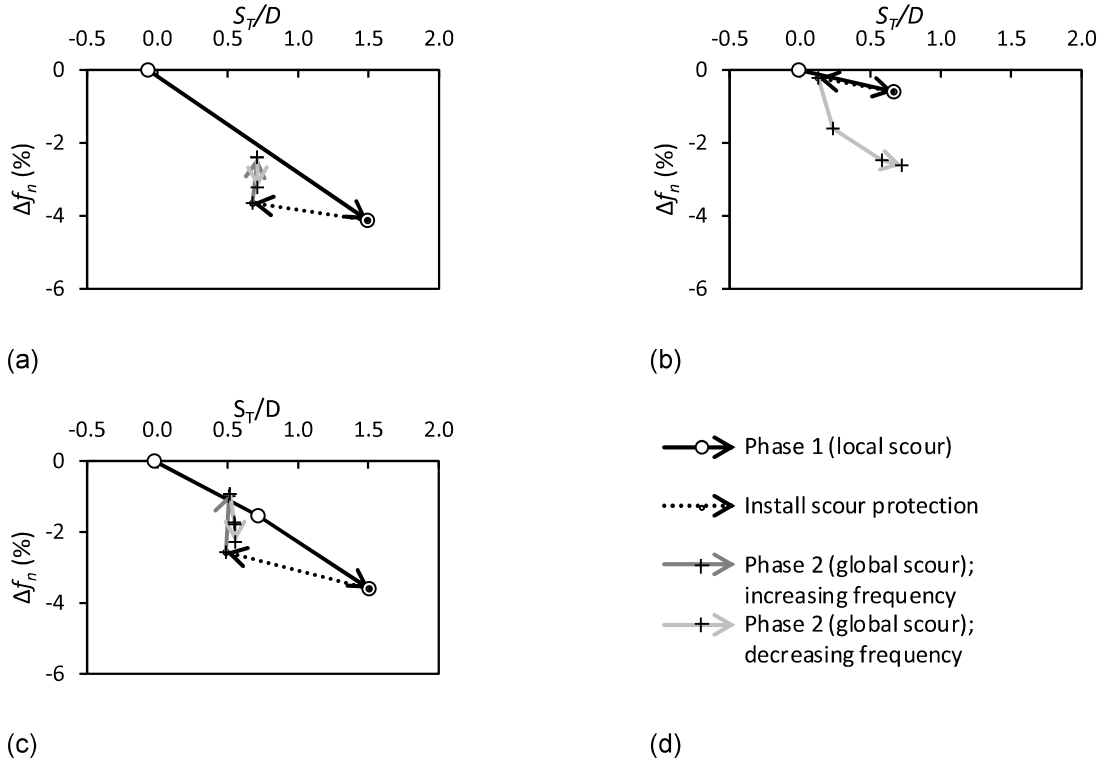

Fig. 19. Mean relative change in mode 1 natural frequency (for N_M = 0, 1, 3, 6) with scour and rock fill remedial scour protection; (a) Test 3; (b) Test 4; (c) Test 6; (d) Legends

736

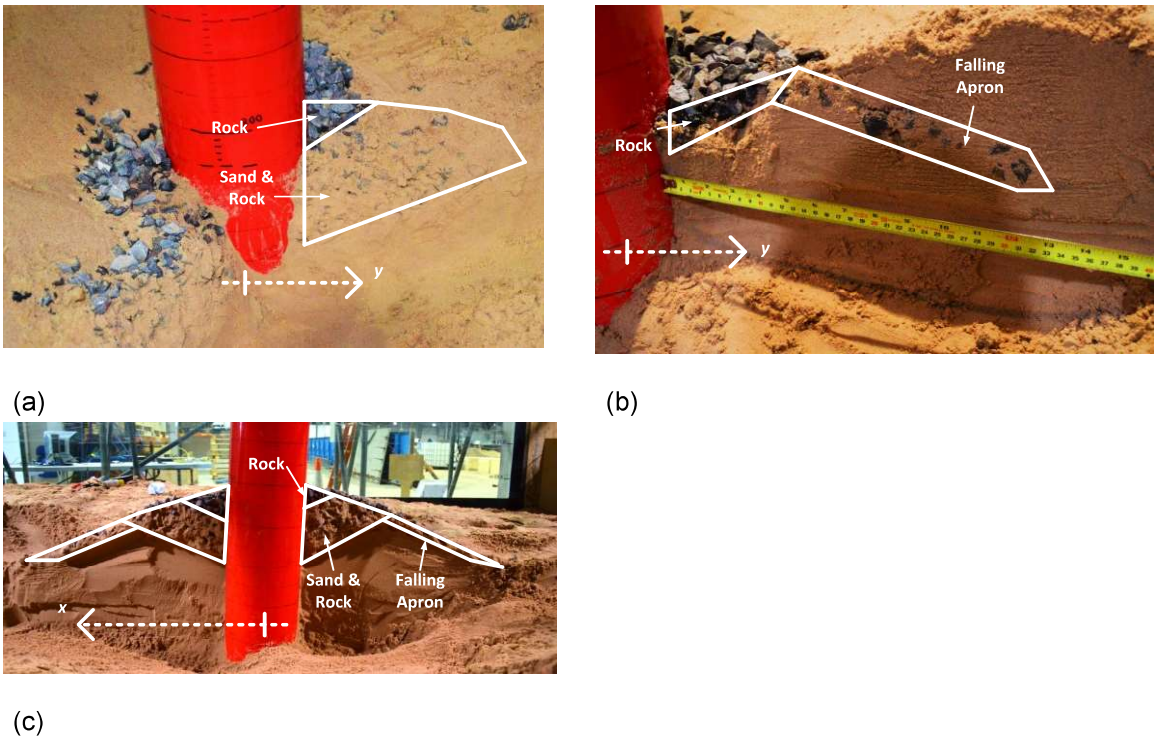

Fig. 20. Photographs of rock scour fill protection cross sections, arrows indicate the flume x and y-axis directions; (a) Test 3 – Rock fill; (b) Test 4 – Rock fill in partial scour hole; (c) Test 6 – Rock fill

737

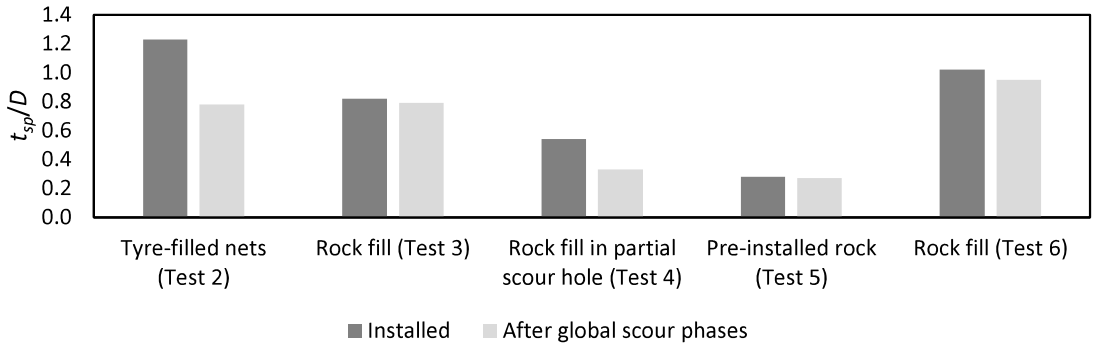

Fig. 21. Change in scour protection thickness adjacent to the pile after global scouring

738

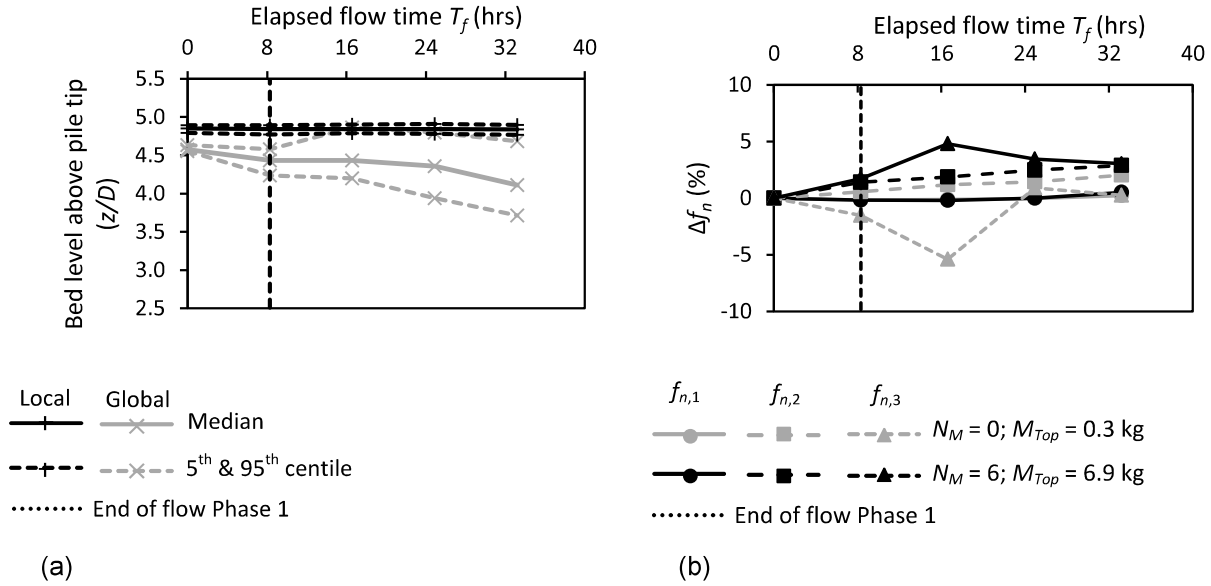

Fig. 22. Experiment results – pre-installed rock armour scour protection (Test 5); (a) Bathymetry outputs; (b) Change in natural frequency

739

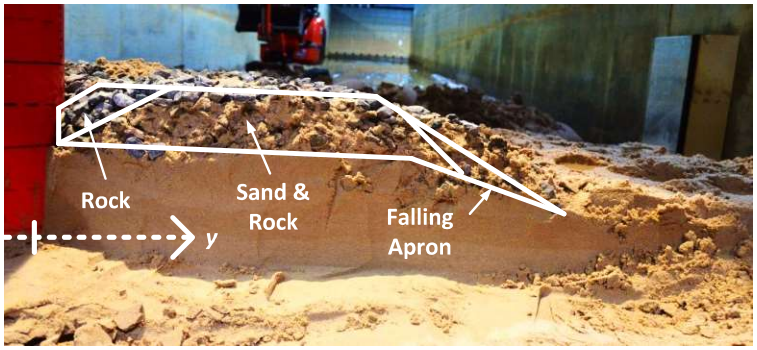

Fig. 23. Photographs of rock scour protection cross sections for Test 5 – pre-installed rock armour, arrow indicates the flume y-axis direction

740